# UNIVERSIDAD COMPLUTENSE DE MADRID

## FACULTAD DE CIENCIAS FÍSICAS

**Máster en Física Teórica**


## TRABAJO DE FIN DE MÁSTER

# Susurros de la oscuridad: Estudio de las transiciones de fase de la materia oscura con ondas gravitacionales

# Whispers from the dark: Probing dark matter phase transitions with gravitational waves

**Jesús Luque del Castillo**

Directores

José Alberto Ruiz Cembranos

Javier Rubio Peña

**Curso académico 2023-24**

# Whispers from the dark: Probing dark matter phase transitions with gravitational waves

Jesús Luque del Castillo and supervisors José Alberto Ruiz Cembranos & Javier Rubio Peña

**Abstract:** In this MSc thesis we consider the *Bubble Expansion* mechanism for the production of dark matter during a first-order phase transition in the early universe. Seeking a dark matter density in agreement with the cosmic microwave background observations, we will study different couplings between the dark matter and the field undergoing the transition, always taking scalar particles. We will see how the larger the dimension of the coupling term in the Lagrangian, the larger the range of allowed values for the parameters. Moreover, this mechanism allows large values for the mass of the dark matter candidate. On the other hand, the gravitational wave spectrum associated with the phase transition is also presented, which could be observed in future experiments in the case of a transition at the electroweak scale, where the model holds in all the cases studied.

## I. INTRODUCTION

Observations of the Cosmic Microwave Background (CMB) point out that we live in a universe dominated by dark energy, with a density parameter $\Omega_\Lambda = 0.685$, while for matter this parameter takes a value $\Omega_\mathrm{M} = 0.316$, of which $\Omega_\mathrm{DM} = 0.265$ is dark matter (DM) [1]. Historically, one of the main evidence of the existence of DM came from the study of galaxy rotation curves during the second half of the 20th century, where it was seen that stars farther away from the galactic nucleus rotated faster than would be expected according to visible mass. This phenomenon was explained by assuming that galaxies are surrounded by a DM halo. Another evidence of DM came from the observation of the deflection of light passing through galaxies, an effect called *gravitational lensing* [2], which could not be explained without the spacetime curvature induced by DM. Furthermore, DM plays a major role in the formation of the *large scale structure* thanks to its gravitational contribution.

The true nature of DM remains a mystery and is one of the unsolved problems of modern physics. There are many candidates of DM like *Weakly Interacting Massive Particles* [3] or *light axions* [4]. Along with them exist a vast variety of DM production's mechanisms as *thermal Freeze-Out* (FO) [5], but most of them present constraints on the mass of the DM candidate. For example, for the FO mechanism, the *unitarity bound* set an upper limit of order $\mathcal{O}(100\mathrm{TeV})$ [6]. Some other models take advantage of the possibility of *First-Order Phase Transitions* (FOPTs) during the early universe [7], a scenario that allows a DM mass heavier than these bounds.

A phase transition (PT) is a discontinuous change in the properties of a system. An *order parameter* distinguishes between the phases, being zero in one of them and non-zero in the other. In a FOPT the order parameter changes discontinuously (usually with temperature) while in a second order PT the order parameter is continuous, its first derivative being discontinuous. One example is the electroweak PT, along with which the early universe may have gone through many other transitions due to its expansion and consequent cooling [8]. In terms of quantum field theory (QFT), in a FOPT the vacuum of the theory changes, since new minima appear in the potential, which are separated by barriers. This allows the universe to be trapped in a minimum of the potential which was formerly a global minimum but at some point turned into a local one. Therefore, the transition is the change from the *false vacuum* to the new global minimum of the potential or *true vacuum*. As a consequence, the field undergoing the transition acquires a non-zero vacuum expectation value (VEV), being this the order parameter, spontaneously breaking the symmetry of the Lagrangian. However, due to thermal fluctuations, the PT does not occur simultaneously at all points in the universe. The regions where the PT has already occurred (VEV$\neq 0$) form bubbles which expand and collide with other bubbles. These collisions, together with the sound waves propagating in the plasma, give rise to a spectrum of gravitational waves (GWs) that could be measured today [8].

In the context of FOPTs, the recently proposed *Bubble Expansion* (BE) mechanism for DM production [9], on which we will focus, presents some appealing features. This model relays on a relativistic expansion of the bubbles with a DM candidate coupled to the FOPT sector, producing an abundance $\Omega_\mathrm{BE}$, which is also known as density parameter, in agreement with the observations and a GW signal potentially observable in future experiments as the Einstein Telescope (ET) [10], Big Bang Observer (BBO) [11] or Laser Interferometer Space Antenna (LISA) [12]. Therefore, the aim of this work is to study this mechanism in the case of scalar particles for different couplings, revisiting the proposal in [9] and introducing others for non-renormalizable Lagrangians, more common in effective field theories. We will be interested in the calculation of the DM abundance, and its pertinent GW spectrum.

This MSc thesis is organized as follows: in Section II we revisit some fundamental aspects about PTs and QFT. In Section III, we introduce the DM production mechanism we are interested in, deriving the DM density parameter for different couplings between the DM candidate and the FOPT sector. In Section IV we present the GW spectrum produced during these transitions and we end in Section V with our conclusions.

## II. THEORETICAL BACKGROUND

The fundamental idea behind the BE mechanism [9] is a coupling between the DM ($\phi$) and the FOPT sector of the form $\sim \phi^m \Phi^n$, with $\Phi$ the field that undergoes the transition. The field is described around $\langle\Phi\rangle$, the VEV, as $\Phi(\mathbf{x}) = h(\mathbf{x}) + \langle\Phi\rangle$, so the interaction can also be expanded around this parameter. Hence, the coupling inside the bubbles will be proportional to $v$, the value of the VEV in the non-symmetric phase. As will be seen, the high-speed expansion of the bubbles leads to a decay of $h$ into the DM candidate that explains the observed abundance. Therefore, it becomes necessary to present some basic aspects about the dynamics of these bubbles and to revisit some notions of QFT and cosmology.

The behavior of the bubbles in PTs is a widely treated and highly complex subject [8, 13, 14]. However, in this work it is not an aspect of great relevance, so it is sufficient to describe it in terms of their characteristic scales. Thus, we will say that the PT begins when the number of bubbles per Hubble volume reaches one, which occurs when the temperature, due to the expansion and cooling of the universe, is lower than the *nucleation temperature*, $T_\mathrm{n}$. From this moment on, expanding bubbles appear. Moreover, during the transition, an amount of energy $\epsilon$ is released, which gives us an idea of the strength of the transition. This energy is parametrized through $\alpha \equiv \epsilon/\rho$, with $\rho$ the energy density of the symmetric phase. The bubbles are defined as the regions in which VEV$\neq 0$, being zero outside them. Nonetheless, this change is not abrupt, since within the bubble wall, of width $L_w$, the expected value varies smoothly from $v$, the value of $\langle\Phi\rangle$ inside the bubbles, to zero. Another parameter of interest will be $\beta$, which is a measure of the inverse of the PT duration, so it is typically expressed in multiples of $H$, the Hubble parameter. Finally, we will call the *final temperature*, $T_\mathrm{f}$, the temperature reached after the transition. Usually $T_\mathrm{f} \gtrsim T_\mathrm{n}$, although in some regimes, such as supercooling [13], $T_\mathrm{f} \gg T_\mathrm{n}$, which usually leads to strong FOPTs where bubbles expand at high velocity.

On the other hand, when studying the decay of a particle into a two particles final state, which will be the case of interest, the probability of transition is given by

$$P_{h\to\phi_1\phi_2} \equiv P \equiv \int \frac{d^3k^{\phi_1} d^3k^{\phi_2}}{(2\pi)^6 2k_0^{\phi_1} 2k_0^{\phi_2}} |\langle h|\mathcal{T}|\phi_1\phi_2\rangle|^2, \quad (1)$$

where $\mathbf{k}_{\phi_1}, \mathbf{k}_{\phi_2}$ are the momenta of the produced particles and where $\mathcal{T}$ can be derived from the matrix element $\mathcal{M}$. In order to compute the latter, one typically turns to Feynman diagrams. If we take a coordinate system in which the expanding bubble wall is at rest, so that the expected value of $\Phi$ varies along the z-axis, it will be the $h$ particles themselves that approach the bubble at wall velocity $v_w$. However, although our system does not depend on time or the momentum components orthogonal to $z$, $\mathbf{p}_\perp$, the wall breaks the invariance at $z$, so $p_z$ is not conserved. Consequently, we will not be able to apply standar Feynman's rules. As an alternative [15], we use

$$\langle h|\mathcal{T}|\phi_1\phi_2\rangle = \int \langle h|\mathcal{H}_{int}|\phi_1\phi_2\rangle = (2\pi)^3 \delta_\perp^2 \delta_0 \mathcal{M}, \quad (2)$$

where $\delta_\perp^2 \equiv \delta^2(p_\perp^h - k_\perp^{\phi_1} - k_\perp^{\phi_2})$, $\delta_0 \equiv \delta(p_0^h - k_0^{\phi_1} - k_0^{\phi_2})$, being $\mathbf{p}^h$ the momentum of the decaying particle and

$$\mathcal{M} = \int dz \chi^*_{\phi_1}(z) \chi^*_{\phi_2}(z) \chi_h(z) V(z), \quad (3)$$

with $V(z)$ the contraction of the interaction Hamiltonian density with all other state information, spinors and polarizations, and $\chi(z)$ a solution to the free particle evolution equation in the presence of the bubble wall [15]. For scalar particles $\chi(z) = \exp(ip_z z)$, so that

$$\mathcal{M} = \int dz e^{i\Delta p_z z} V(z), \quad (4)$$

being $\Delta p_z = p_z^h - p_z^{\phi_1} - p_z^{\phi_2}$.

Once $\mathcal{M}$ is known, the decay probability can be computed as usual via eq. (1), an expression that in the regime $(p_0^h)^2 \gg m_h^2 (\implies p_0^h \simeq p_z^h)$ reduces to [15]

$$P = \frac{1}{2p_0} \int \frac{d^3k^{\phi_1} d^3k^{\phi_2}}{(2\pi)^6 2k_0^{\phi_1} 2k_0^{\phi_2}} (2\pi)^3 \delta_\perp^2 \delta_0 |\mathcal{M}|^2. \quad (5)$$

With this result at hand, it is possible to derive the density of the DM produced [9] as

$$n_\phi \simeq \frac{2}{\gamma_w v_w} \int \frac{d^3p^h}{(2\pi)^3} P(h\to\phi^2) e^{-\frac{\gamma_w (E_h - v_w p_z^h)}{T_\mathrm{n}}}, \quad (6)$$

where $\gamma_w$ is the Lorentz's factor and $E_h$, the energy of the decaying particle, $h$. Finally, the associated actual abundance is given by the energy density multiplied by a factor that accounts for its dilution due to the expansion of the universe

$$\Omega_\mathrm{BE} h^2 = h^2 \frac{M n_\phi}{\rho_c} \frac{g_{\star s0} T_0^3}{g_{\star s}(T_\mathrm{f}) T_\mathrm{f}^3}, \quad (7)$$

with $\rho_c = 3H_0^2/8\pi G$ the critical energy density, $T_0$ the temperature today and $g_{\star S0}/g_{\star S}(T_\mathrm{f})$ is the entropy number of degrees of freedom today/at the final temperature. Note that, in this occasion, $h$ is the dimensionless Hubble parameter.

Finally, we introduce some basics about GWs. In the PT context, there are two main sources of GWs: the *scalar field* contribution and the *sound waves* contribution [16–18]. During the transition, the VEV of the field involved varies smoothly through the bubble wall, inducing shear stresses that accumulate kinetic energy from the expansion. This energy is released in the form of GW when the bubbles collide. This is the so-called *scalar field* or *bubble collision* contribution. Besides, the transfer of energy from $h$ to the plasma due to friction gives rise to sound waves, which are another source of GWs. Thus, two cases are distinguished: the *terminal velocity*

regime, in which the friction is sufficient to slow down the bubble wall so that it reaches a constant velocity, and the *runaway* regime, in which the energy released is such that the wall continues to accelerate until collision, reaching ultra-relativistic velocities. In both cases the GW spectrum depends on the parameters already presented $(\alpha, \beta, v_w, T_\mathrm{f})$.

## III. BE MECHANISM

We consider a model in which all the particles involved are scalar particles. When the PT takes place, $\Phi$ acquires a non-zero VEV, giving rise to expanding bubbles as already described. The BE itself can excite degrees of freedom of mass up to $M \sim \sqrt{\gamma_w} T_\mathrm{n}$, producing heavy particles [19], that could play the role of DM ($\phi$). Thus, we will study the following non-renormalizable effective Lagrangian, which describes the system at energies below the $\Lambda$ scale and where the potential $V(\Phi)$ is not specified in order to keep the greatest possible generality,

$$\mathcal{L} = \frac{(\partial_\mu \Phi)^2}{2} + \frac{(\partial_\mu \phi)^2}{2} - \frac{M^2\phi^2}{2} - \frac{\lambda \phi^2 \Phi^n}{n\Lambda^{n-2}} - V(\Phi). \quad (8)$$

The dimensionless coupling constant, $\lambda$, will play a major role in this expression in the renormalizable case ($n = 2$), where the Lagrangian is valid for all energy scales, needing small values to allow a perturbative treatment. Furthermore, in the non-renormalizable cases ($n \neq 2$), $\Lambda$ is the energy scale up to which the effective field theory is valid, so the rest of the parameters must take values lower than this one. On the other hand, expanding around the VEV and taking the leading order, the interaction term takes the form $\lambda \langle\Phi\rangle^{n-1} \phi^2 h / \Lambda^{2-n}$, producing a $h \to \phi\phi$ decay. As already stated, the VEV varies along the wall from 0 on the symmetric side to $v$ on the non-symmetric one. To simplify the calculations, since it hardly affects the final result, we will assume that this change is linear, so that $\langle\Phi\rangle = vz/L_w$ within the wall.

Moreover, if we take the discussed frame we can use the following kinematics

$$\begin{aligned} p^h &= (p_0, 0, 0, \sqrt{p_0^2 - m_h^2}) \\ k^{\phi_1} &= (p_0(1-x), 0, k_\perp, \sqrt{p_0^2(1-x)^2 - k_\perp^2 - M^2}) \\ k^{\phi_2} &= (p_0 x, 0, -k_\perp, \sqrt{p_0^2 x^2 - k_\perp^2 - M^2}), \end{aligned} \quad (9)$$

with $x \in [0,1]$, so the energy is conserved.

Furthermore, for scalar particles $V(z) = \lambda \langle\Phi\rangle^{n-1} / \Lambda^{n-2}$, so that

$$V(z) = \begin{cases} 0, & \text{if} \quad z < 0 \\ \frac{\lambda}{\Lambda^{n-2}} (v \frac{z}{L_w})^{n-1}, & \text{if} \quad 0 < z < L_w \\ \frac{\lambda}{\Lambda^{n-2}} v^{n-1}, & \text{if z} > L_w \end{cases} . \quad (10)$$

Finally, a quantity of interest will be $\Delta p_z$, which taking $p_0^2(1-x)^2 \gg k_\perp^2 + M^2$ and $p_0^2 x^2 \gg k_\perp^2 + M^2$ reduces to

$$\Delta p_z \simeq \frac{k_\perp^2 + M^2}{2p_0 x(1-x)}. \quad (11)$$

This limit simplifies the calculations while, from a physical point of view, it stands for a large value of $p_0$, consistent with a relativistic expansion of the bubbles, and prevents one of the two particles produced from taking almost all the energy ($x \simeq 0, x \simeq 1$).

Once the model has been presented we will revisit the renormalizable case. Then we will study $n = 3, 4$, where the Lagrangian is non-renormalizable, this being the general case for an effective field theory.

### A. Four-dimensional interaction ($n = 2$)

We begin with the case $n = 2$, this being the one already treated in [9]. We will take advantage of the fact that it is the simplest model to present more details about the calculation. This way, the interaction term of the Lagrangian is reduced to $\mathcal{L}_\mathrm{int} = \lambda \langle\Phi\rangle h \phi^2$. As the Lagrangian is renormalizable, the description is valid at all scales, so the cut-off scale is not necessary.

$\mathcal{M}$ is computed via eq (4), taking eq. (10) as a prescription of V(z). Consequently

$$\mathcal{M} = \lambda v (e^{i\Delta p_z L_w} - 1)/(L_w \Delta p_z^2), \quad (12)$$

expression from which it can be derived that

$$|\mathcal{M}|^2 = \left(\frac{\lambda v}{\Delta p_z}\right)^2 \left(\frac{\sin(\alpha)}{\alpha}\right)^2; \quad \alpha = \frac{L_w \Delta p_z}{2}. \quad (13)$$

Once the matrix element has been determined, we are ready to compute the decay probability, making use of eq. (5). If this result is substituted in eq. (5), as well as the 0 component of the momenta, shown in eq. (9), the probability is rewritten as

$$P = \frac{1}{2p_0} \frac{\lambda^2 v^2}{(2\pi)^3} \int \frac{d^3 k^{\phi_1}}{2p_0 x} \frac{d^3 k^{\phi_2}}{2p_0(1-x)} \delta_\perp^2 \delta_0^2 \frac{\mathrm{sinc}^2(\alpha)}{\Delta p_z^2}. \quad (14)$$

Notice how the dependence in the transversal components is quadratic, being also $k_\perp^{\phi_1} = -k_\perp^{\phi_2}$, so that $(k_\perp^{\phi_1})^2 = (k_\perp^{\phi_2})^2 \equiv k_\perp^2$. Thus, we can integrate over $d^2\mathbf{k}_\perp^{\phi_2}$ with the associated Dirac delta. In addition, we change $d^3 k^{\phi_1}$ to cylindrical coordinates, which allows us to rewrite the former equation as

$$P = \frac{1}{2p_0} \frac{\lambda^2 v^2}{(2\pi)^2} \int \frac{dk_z^{\phi_1} |\mathbf{k}_\perp^{\phi_1}| dk_\perp^{\phi_1}}{4p_0^2 x(1-x)} dk_z^{\phi_2} \delta_0 \frac{\mathrm{sinc}^2(\alpha)}{\Delta p_z^2}. \quad (15)$$

The calculation simplifies if we integrate in $x, k_\perp^2, k_0^{\phi_1}$. To carry out this change of variables we introduce the associated Jacobian, $J = k_0^{\phi_1} p_0^2 x / (2 k_z^{\phi_1} k_z^{\phi_2} k_\perp)$. If we make

this change and use the remaining Dirac delta, the probability becomes

$$P \simeq \frac{\lambda^2 v^2}{16\pi^2}\int \frac{dx\, dk_\perp^2\, x(1-x)}{(k_\perp^2+M^2)^2}\mathrm{sinc}^2(\alpha)\Theta(p_0-2M). \quad (16)$$

where the Heaviside function comes from the necessity that the $z$ component of the momenta must be real. We also have considered again the limit $p_0^2(1-x)^2 \gg k_\perp^2+M^2$ and $p_0^2x^2 \gg k_\perp^2+M^2$, so that $k_z^{\phi_1}k_z^{\phi_2} \simeq p_0^2x(1-x)$.

Finally, since the function $\mathrm{sinc}^2(x)$ goes quickly to 0 for $x \gg 1$ and has a value close to 1 otherwise, we impose that $\alpha \lessapprox 1$, or equivalently, $p_0 - M^2L_w > 0$, so we replace this function by a new step function $\Theta(p_0 - M^2L_w)$, which leads us to

$$P = \frac{1}{4}\frac{\lambda^2 v^2}{24\pi^2 M^2}\Theta(p_0-2M)\Theta(p_0-M^2L_w). \quad (17)$$

This expression corrects the result of [9] by a factor 1/4. Moreover, $L_w \sim 1/v$ [9], so that, taking the hierarchy $M \gg v$ (valid for heavy candidates), we have that $M^2L_w > 2M$.

Now that we have an expression for the probability of decay, $P$, we can compute the DM's density through eq. (6) and then the density parameter, given by eq. (7). Computing eq. (6) in cylindrical coordinates, and taking $p_z \gg M$ (consequent with the relativistic expansion) it is easily derived that

$$n_\phi = \frac{\lambda^2 v^2}{384\pi^4 M^2 \gamma_w v_w}\int_0^\infty dp_\perp^2 \int_{M^2/v}^\infty dp_z e^{-\frac{\gamma_w}{T_\mathrm{n}}\sqrt{p_z^2+p_\perp^2}-v_w p_z}, \quad (18)$$

from which it finally follows that the DM density produced is

$$n_\phi = \frac{1}{4}\frac{\lambda^2 v^2 T_\mathrm{n}^2}{48\pi^4 M^2\gamma_w^3 v_w} e^{-\frac{\gamma_w}{T_\mathrm{n} v}M^2(1-v_w)} \times\left[\frac{M^2/v}{1-v_w}+\frac{(2-v_w)T_\mathrm{n}}{(1-v_w)^2\gamma_w}\right]. \quad (19)$$

In the ultra-relativistic limit ($\gamma_w \gg 1$), the previous equation reads as

$$n_\phi = \frac{1}{4}\frac{\lambda^2 v^2 T_\mathrm{n}^3}{12\pi^4 M^2} e^{-\frac{M^2}{2T_\mathrm{n} v\gamma_w}}. \quad (20)$$

Since we are taking $\gamma_w \to \infty$ we can also drop the exponential.

Finally, we derive an expression for the today's DM density parameter in this regime,

$${}^2\Omega_{BE}h^2 = 2.7\cdot 10^7 \frac{\lambda^2}{g_{\star s}}\frac{v}{M}\frac{v}{200\,\mathrm{GeV}}\left(\frac{T_\mathrm{n}}{T_\mathrm{f}}\right)^3, \quad (21)$$

where the superscript 2 stands for $n = 2$. So far, we have obtained an analytic expression for the density parameter of the DM produced by the expansion of nucleated bubbles in a PT. To do this we have taken $p_0 \simeq p_z \gg M$, consistent with the high speed expansion, as well as

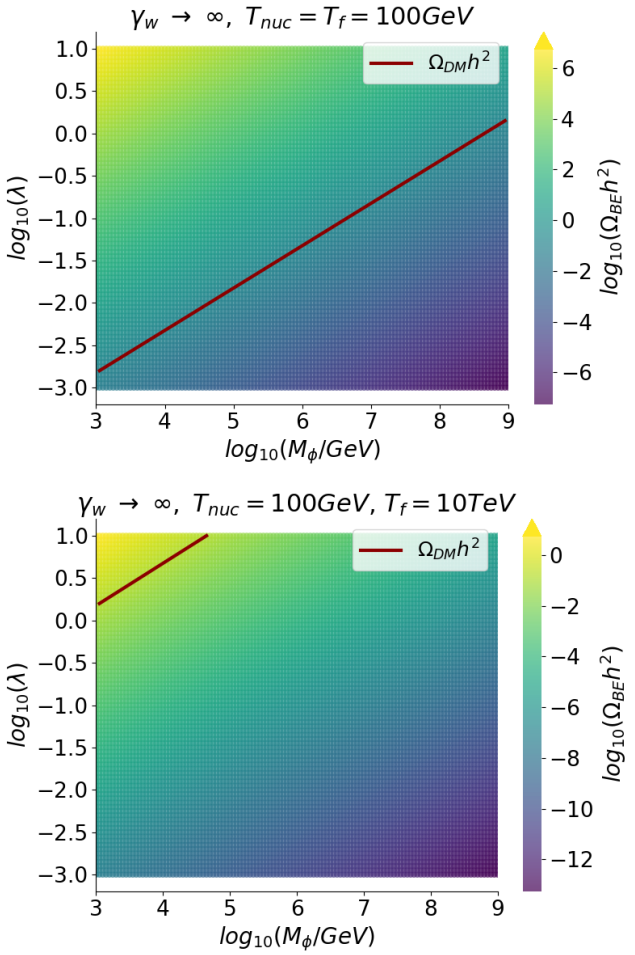


FIG. 1. The density parameter for the model $n = 2$ in the ultra-relativistic limit for $v = 200$ GeV and for $T_\mathrm{f} = 100$ GeV (upper panel) and $T_\mathrm{f} = 10$ TeV (lower panel). The red line stands for the points in agreement with the observational value, $\Omega_\mathrm{DM}h^2 = 0.1200 \pm 0.0012$.

$p_0^2(1-x)^2 \gg k_\perp^2+M^2$ and $p_0^2x^2 \gg k_\perp^2+M^2$, i.e., $x$ must be such that the energy of the two produced particles is of the same order. We now study the parameter space, in order to determine which values are in agreement with the observational value, $\Omega_\mathrm{DM}h^2 = 0.1200 \pm 0.0012$ [1].

As seen in the upper panel of Figure 1, taking parameter values on the electroweak scale we achieve a DM production in agreement with the observations for a wide range of $\lambda$ values, which in addition allows high masses of the DM candidate, typically forbidden in other production's mechanisms [6]. However, the model has a strong dependence on the final temperature. The higher this temperature the lower the abundance, which means that the parameter space in agreement with the observations is much smaller, as can be seen in the lower panel of the Figure 1. Mathematically, for $T_\mathrm{f} > 100T_n$ we would not find parameter values for which production would be sufficient. Nonetheless, these regimes are not usually found in PTs. Moreover, if the expansion is non-relativistic,

the production is strongly suppressed, as seen in eq. 19, being also insufficient. It is important to note that we are always considering values of the coupling constant at most of order one, so the theory remains perturbative. Thus, the parameter space in the bottom panel of Figure 1 is even more constrained. Likewise, since we are interested in massive DM we have not consider masses below the TeV scale.

Therefore, it is found that the BE mechanism in its simplest version for scalar fields allows a DM production that agrees with the observations, allowing in addition to have a heavy DM candidate. Nevertheless, the model is constrained to some extent by the bubble expansion velocity, while for final temperatures higher than the nucleation temperature the parameter space in agreement with the observations is highly reduced. Consequently, we now discuss more general cases, which may allow more freedom in the parameters.

### B. Five-dimensional interaction ($n = 3$)

Once we have studied the renormalizable case for the BE mechanism we will consider a non-renormalizable Lagrangian, which is usual for effective theories. This way, the interaction term is $\mathcal{L}_{\rm int} = \lambda\langle\Phi\rangle^2 h\phi^2/\Lambda$, where let us recall that $\Lambda$ is the energy scale up to which the theory is valid, thus being the parameter with the largest value. In this sense, the coupling constant, $\lambda$, loses its meaning, since it is $\lambda/\Lambda$ that plays his role, so we fix $\lambda = 1$. Again, we are interested in computing the abundance of DM produced, for which we will carry out a process analogous to the previous one.

First, we calculate the matrix element $\mathcal{M}$ through eq. (4), being the function $V(z)$ given by eq. (10), so that

$$|\mathcal{M}|^2 = \left(\frac{2\lambda v^2}{\Lambda(\Delta p_z)^3 L_w^2}\right)^2 \times \left(L_w^2\Delta p_z^2 + 4\sin^2(\alpha) - 2\sin(\beta)\Delta p_z L_w\right), \tag{22}$$

where $\alpha = \Delta p_z L_w/2$ and $\beta = \Delta p_z L_w$. With this expression, we can now derive the probability via eq. (5). Before doing so, it is convenient to introduce factors $\Delta p_z L_w/\Delta p_z L_w$ to have functions $\mathrm{sinc}(\alpha(/\beta))$. Then, we follow the same steps as before, making the same assumptions and changes of variables to obtain

$$P = \frac{1}{(2\pi)^2}\frac{\lambda^2 v^4}{\Lambda^2 L_w^4}\Theta(p_0 - 2M)\times \left[\frac{p_0^2 L_w^2}{105M^6}\left(1 + \Theta(a) - 2\Theta(b)\right) + \frac{L_w^4}{18M^2}\Theta(b)\right]. \tag{23}$$

with $a = (p_0 - M^2 L_w)$, $b = (p_0 - 2M^2 L_w)$. Taking again $M \gg v$ [9], we have that $2M^2 L_w > M^2 L_w > 2M$, which relates the arguments of the Heaviside functions.

Once the probability is known we can derive the density via eq. (6) and then the abundance through eq. (7).

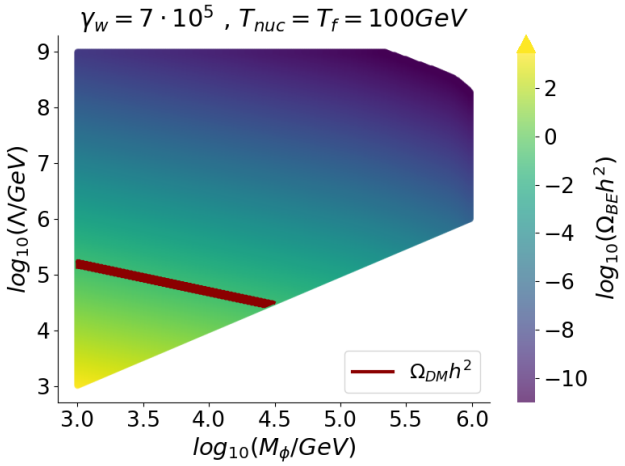


FIG. 2. Same as for the upper panel in Figure 1 but for $n = 3$ and $\gamma_w = 7\cdot 10^5$.

Due to its complexity, we present the complete expression in Table I, which, in the ultra-relativistic limit, taking only the leading order, reduces to

$${}^3\Omega_{\rm BE}h^2 \simeq 7.4\cdot 10^7 \frac{\lambda^2\gamma_w}{g_{\star s}}\frac{T_{\rm n}^4 v^5}{T_{\rm f}^3\Lambda^2 M^4}\frac{v}{200\,\mathrm{GeV}}\left(\frac{3M}{2v} - 1\right). \tag{24}$$

It is important to point out that the expression obtained is always positive, since in the process followed we have always considered $M \gg v$. Otherwise, the expression we have arrived at would be different, since there would be a different relationship between the Heaviside functions, but also positive as expected. Moreover, unlike for the result for the case $n = 2$, seen in eq. (21), even in the ultra-relativistic limit the density parameter depends on the Lorentz's factor.

Therefore, we explore in Figure 2 the parameter space of the expression (24) for parameters associated with a PT on the electroweak scale. When studying the values that are in agreement with the observations we will make use of the complete expression for ${}^3\Omega_{BE}h^2$ presented in Table I. We see how the parameter space is more restricted. To a large extent this is due to the higher dependence on $M$, which reduces the DM production. The lower cut is for $\Lambda = M$. However, unlike the previous case, we find agreement with the observations without the need to have an expansion of the bubble wall at ultra-relativistic velocities, which was a constraint in the $n = 2$ case. Furthermore, thanks to the dependence on $\gamma_w$ seen in eq. (24), for ultra-relativistic velocities the model holds for large values for the DM mass while the impact of $T_{\rm f}/T_n$ is reduced.

On the other hand, it is interesting to consider values on scales other than the electroweak, and also different values of $T_{\rm f}$, for which, in Figure 3, we represent only those values in agreement with the observations. First, we can check in this graphic how $\gamma_w$ compensates for the decrease in production caused by large values of the mass

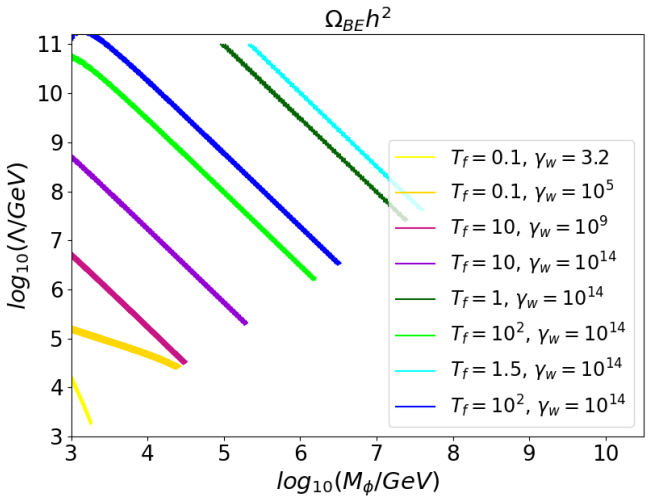


FIG. 3. The density parameter for different conditions. $T_{\rm f}$ shown are in TeV. The yellow lines are for $v = 200\,\text{GeV}$ and $T_{\rm n} = 100\,\text{GeV}$, as well as the purple/pink ones. The green lines are for $v = T_{\rm n} = 1\,\text{TeV}$ and the blue ones for $v = T_{\rm n} = 1.5\,\text{TeV}$.

or final temperature. Actually, it is strictly possible to have values for $M$ and $T_{\rm f}$ as high as we want since we can always compensate them taking $\gamma_w \to \infty$. On the other hand, we see how transitions in which the VEV acquired is larger, as well as the nucleation temperature, allow for more massive DM candidates and a larger range of parameters in agreement with the observations, especially for ultra-relativistic velocities.

Therefore, the main difference between this non-renormalizable case and the one initially proposed in [9] and reviewed above ($n = 2$) is that, even in the relativistic limit, the density parameter obtained depends on the wall velocity, which allows a wider range of DM's masses.

### C. Six-dimensional interaction ($n = 4$)

Finally, we study an interaction term of the Lagrangian $\mathcal{L}_{\rm int} = \lambda\langle\Phi\rangle^3 h\phi^2/\Lambda^2$, being also non-renormalizable. For the same reason as before, we will take again $\lambda = 1$. The study of this case will allow us to determine how affects the type of dependence on the VEV and the cut-off scale, giving an idea of the behavior in the more general case shown in eq. (8).

Again, we seek to obtain the DM density parameter. To do this we will follow the same procedure as before, taking the same considerations where necessary. Thus, first we compute the matrix element $\mathcal{M}$ through eq. (4), being $V(z)$ given by eq. (10), so we have that

$$\mathcal{M} = \frac{\lambda v^3}{\Lambda^2 L_w^3}\left[\frac{6}{\Delta p_z^4} + e^{i\Delta p_z L_w}\left(\frac{6iL_w}{\Delta p_z^3} - \frac{6}{\Delta p_z^4} + \frac{3L_w^2}{\Delta p_z^2}\right)\right]. \tag{25}$$

This equation give rise to

$$|\mathcal{M}|^2 = \left(\frac{\lambda v^3}{L_w^3\Lambda^2\Delta p_z^4}\right)^2\Big[144\sin^2\alpha + 9\Delta p_z^4 L_w^4 - 72L_w^2\Delta p_z^2\sin^2\alpha + 36\Delta p_z^2 L_w^2 - 72\Delta p_z L_w\sin\beta\Big], \tag{26}$$

Knowing the squared amplitude we can determine the decay probability via eq. (5). To do so, we change coordinates to integrate at $x, k_\perp^2, k_0^{\phi_1}$ and consider again $p_0^2(1-x)^2 \gg k_\perp^2 + M^2$ and $p_0^2 x^2 \gg k_\perp^2 + M^2$. Thus, we derive the probability sought,

$$\mathcal{P} = \frac{\pi}{70(2\pi)^3}\frac{\lambda^2 v^6}{\Lambda^4 L_w^6}\Theta(p_0 - 2M)\Big[3\frac{p_0^2 L_w^4}{M^6}\big(1 - 2\Theta(a) + \frac{4}{3}\Theta(b)\big) + \frac{16}{11}\frac{L_w^2 p_0^4}{M^{10}}\left(1 + \Theta(a) - 2\Theta(b)\right)\Big], \tag{27}$$

with $a = (p_0 - M^2 L_w)$ and $b = (p_0 - 2M^2 L_w)$. Recalling that $M \gg v \simeq 1/L_w$, we have again the same relation between the arguments of the Heaviside functions.

With the probability at hand we now derive the density, using eq. (6), result that leads us directly to the density parameter as shown in eq. (7). Once again, the integral we have to perform to compute the density gives rise to an expression with several terms, as well as for the density parameter presented in Table I. Thus we present the ultra-relativistic limit, in which, taking the leading order, ${}^4\Omega_{\rm BE}h^2$ reduces to

$${}^4\Omega_{\rm BE}h^2 \simeq 2.8\cdot 10^9\frac{\lambda^2\gamma_w^3}{g_{\star s}}\frac{v^9 T_{\rm n}^6}{M^8\Lambda^4 T_{\rm f}^3}\frac{v}{200\,\text{GeV}}\left(\frac{3M}{2v} - 1\right), \tag{28}$$

equation with a larger dependence in $\gamma_w$ than in the former case and always positive, as previously discussed.

The dependence on $T_{\rm n}$ is given by the calculation of $n_\phi$ from the probability, which is different for each $n$, while the dependence on $T_{\rm f}$ is always the same, since this appears when calculating the abundance via (7). This way, the higher is $n$, the greater is the dependence on $T_{\rm n}$, being thus smaller the impact of $T_{\rm f} > T_{\rm n}$. On the other hand, the larger the $n$ the greater the mass dependence, which reduces the possibility of having a heavy DM candidate. Nevertheless, in spite of this, we can overcome this restriction with an ultra-relativistic wall thanks to the dependence on $\gamma_w$, being this dependence greater the greater the $n$.

We now study the parameter space in agreement with the observations. For that, we begin taking the parameters in the electroweak scale and using for the calculations the equation presented in Table I. In Figure (4), we see how the parameter space in agreement with the observations, under the same conditions as in the previous cases, allows a wider range of values for both $\Lambda$ and $M$. However, the masses are of the order of the unitarity bound, not being able to exceed it under the conditions presented. Once again, the lower cut in Figure 4 stands for $M = \Lambda$.

| | |
|---|---|
| $^3\Omega_{\rm BE}h^2 = A'\left[\frac{1}{(1-v_W)^4}\left(f_1(2M)+f_1(M^2/v)-2f_1(2M^2/v)\right)+\frac{1}{(1-v_w)^3}\left(f_2(2M)\right.\right.$ $\left.\left.+f_2(M^2/v)-2f_2(2M^2/v)\right)\right]+B'\left(\frac{2M^2}{v(1-v_w)}\frac{\gamma_w}{T_{\rm n}}+\frac{(2-v_w)}{(1-v_w)^2}\right)e^{-\frac{\gamma_w 2M^2(1-v_w)}{T_{\rm n}v}}$ | $A' = \frac{1.54\cdot10^6\lambda^2}{\gamma_w^6 v_w g_{\star s}}\frac{T_{\rm n}^5}{T_{\rm f}^3\Lambda^2}\frac{v^5}{M^5}v_{200}$ <br> $B' = \frac{8.98\cdot10^6\lambda^2}{\gamma_w^4 v_w g_{\star s}}\frac{T_{\rm n}^3}{T_{\rm f}^3}\frac{v^3}{M\Lambda^2}v_{200}$ |
| $^4\Omega_{\rm BE}h^2 = A\left[\frac{1}{(1-v_w)^4}\left(f_1(2M)-2f_1(M^2/v)+\frac{4}{3}f_1(2M^2/v)\right)+\frac{1}{(1-v_w)^3}\left(f_2(2M)\right.\right.$ $\left.\left.-2f_2(M^2/v)+\frac{4}{3}f_2(2M^2/v)\right)\right]+B\left[\frac{1}{(1-v_w)^6}\left(f_3(2M)+f_3(M^2/v)\right.\right.$ $\left.\left.-2f_3(2M^2/v)\right)+\frac{1}{(1-v_w)^5}\left(f_4(2M)+f_4(M^2/v)-2f_4(2M^2/v)\right)\right]$ | $A = \frac{3.47\cdot10^6\lambda^2}{g_{\star s}v_w\gamma_w^6}\frac{T_{\rm n}^5}{M^5}\frac{v^4}{\Lambda^4}\frac{v^3}{T_{\rm f}^3}v_{200}$ <br> $B = \frac{1.42\cdot10^6\lambda^2}{g_{\star s}\gamma_w^8 v_w}\frac{T_{\rm n}^7}{\Lambda^4 T_{\rm f}^3}\frac{v^9}{M^9}v_{200}$ |

$$f_n(x) = \left[\sum_{i=0}^{j}\left(\frac{\gamma_w}{T_{\rm n}}(1-v_w x)\right)^i\frac{j!}{i!}\right]e^{-\frac{\gamma_w}{T_{\rm n}}(1-v_w)x}$$

with $j=3$ for $n=1$, $j=2$ for $n=2$, $j=5$ for $n=3$ and $j=4$ for $n=4$.

TABLE I. Complete expressions of the density parameter for $n=3$ and $n=4$. $v_{200}$ stands for the VEV on the non-symmetric side of the wall normalized by 200 GeV, $v_{200} = v/(200\text{GeV})$.

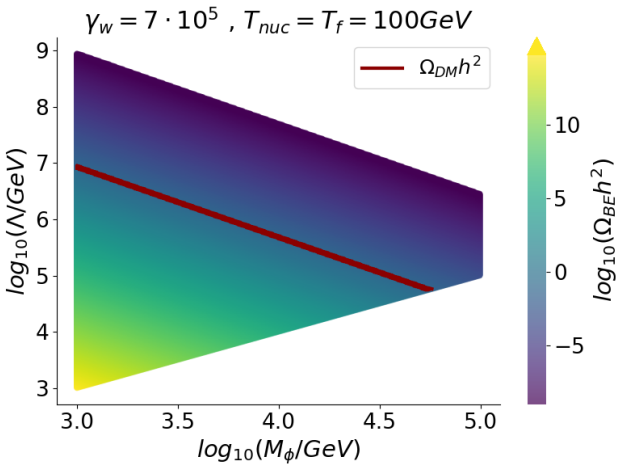


FIG. 4. Same as for the upper panel in Figure 1 but for $n=4$ and $\gamma_w = 7\cdot10^5$.

On the other hand, it is interesting to deal with the effect of the final temperature as well as other values of the VEV and the nucleation temperature, for which we represent in Figure 5 only those values in agreement with the observations. For this purpose, we will make use of ultra-relativistic velocities, studying how the dependence in $\gamma_w$ compensates for large values of $M$, allowing again superheavy candidates. Note that the presented results are also derived using the expression for the abundance in Table I.

Thus, in Figure 5 we present the same cases discussed in the previous subsection. Again, we verify how an ultra-relativistic bubble wall velocity allows a wide range of possibilities for the parameters. Likewise, we have again that for higher values of $v$ and $T_{\rm n}$ the DM production is higher. Moreover, we can see how, in comparison with the case $n=3$, this model allows larger masses and a wider range of $\Lambda$ values, which is due to the greater dependence in $\gamma_w$ and $T_{\rm n}$. This way, being more dependent on $\gamma_w$, it compensates more easily large masses of the DM candidate, so we would find the possibility of agreement with the observations for large values of this magnitude. In addition, the larger range for $\Lambda$ points out that the model is valid up to a larger scale of energies.

So far, we have observed a general behavior for the abundance as $n$ increases. First, the dependence on $T_n$ increases, favoring production and decreasing the negative impact of a final temperature $T_{\rm f} \gg T_n$, which can occur in certain regimes. However, the weight of $M$ in the denominator also increases, which a priori reduces the possibility of massive candidates. Nonetheless, in the non-renormalizable cases we find an increasing dependence on $\gamma_w$, which allows large values of the mass for relativistic velocities (even above the unitarity bound), as well as a validity of the model up to a higher energy scales. Therefore, the larger $n$ is, the greater the range of possible PTs compatible with this mechanism. Moreover, all these tendencies can be expected to continue for larger $n$ so there will come a point where the dependence on $\gamma_w$ will be such that the ultra-relativistic regime will

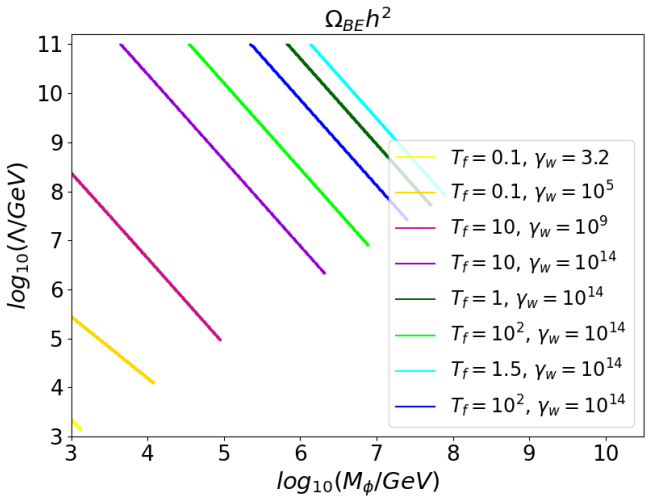


FIG. 5. Same as for Figure 3 but for $n = 4$.

be excluded, since it will always lead to overproduction.

Finally, it should be noted that the BE mechanism may occur along with other mechanisms of DM production, so that the resulting density parameter may be modified [9]. First, if $T_{\rm f} > M$ and the $\phi$ field is coupled to the thermal bath, it may result in production by *Freeze-Out*, a mechanism that in certain regions of the parameter space could give rise to a relevant contribution that should be considered together with that of BE. On the other hand, the coupling between $\phi$ and $h$ can give rise to $\phi$ and $h$ annihilation, which reduces the density of DM produced. These phenomena, along with others, may contribute to the value of $\Omega_{\rm DM}h^2$, modifying the parameter space in agreement with the observations.

## IV. GWS SIGNAL

One of the most interesting features of this DM production mechanism, based on a PT, is the production of GWs. This gives rise to a signal that we can measure today, which could serve as indirect evidence of it. GWs in FOPT have been a widely studied topic in recent years, so that the understanding of them is essentially due to hydrodynamic and scalar field simulations [16–18, 20, 21]. Thus, there are three contributions to this gravitational wave spectrum: the *scalar field* contribution due to collisions between bubbles, the *sound waves* contribution due to sound waves generated by the energy transfer from $h$ to the plasma, and a *turbulent* contribution due to nonlinear effects in the turbulent motion of the plasma. However, due to the large uncertainties it presents and since it is expected to be subdominant [17], we will not consider the turbulent contribution . Relative to the weight of the two remaining contributions we have two parameters, $k_{\rm wall}$ and $k_{\rm fluid}$, which govern the energy distribution between the wall motion and the plasma excitation, so that $k_{\rm wall} = E_{\rm wall}/E_{\rm total}$, $k_{\rm wall} + k_{\rm fluid} = 1$, being $E_{wall}$ the the wall kinetic energy.

As previously discussed, we distinguish between two regimes: the *runaway* regime, in which the bubble wall velocity is ultra-relativistic, and the *terminal velocity* regime, in which the wall reaches a constant velocity. In the latter, only sound waves contribute since once the terminal velocity is reached the portion of the energy stored in the wall starts to decrease as the inverse of the bubble radius, so that $k_{\rm fluid} = 1$. On the other hand, in the former case $k_{\rm wall} = 1 - \alpha_\infty/\alpha$, with $a_\infty$ the value of $\alpha$ from which we are in the runaway regime [22]. Thus, both contributions are important in this case.

First, we present the *scalar field* or *bubble collision* contribution. From numerical calculations it can be obtained that this GW spectrum corresponds to [18]

$$\frac{d\Omega_\phi h^2}{dln(f)} = 4.7\cdot 10^{-8}\left(\frac{100}{g_{*s}}\right)^{1/3}(H_{\rm f}R_*)^2\left(\frac{k_{\rm wall}\alpha}{1+\alpha}\right)^2 S_{\rm wall}, \tag{29}$$

where $g_{*s}$ is evaluated at the time of GWs generation, $H_{\rm f}$ is the Hubble parameter evaluated at the final temperature and $R_*$ is the size of the bubble at the collision, which is computed from the $\beta$ parameter as follows:

$$R_* = \frac{(8\pi)^{1/3}v_w}{\beta}. \tag{30}$$

Finally, $S_{\rm wall}$ is the numerical fit to the spectral function

$$S_{\rm wall} = \frac{(a+b)^c f_p^b f^a}{(bf_p^{\frac{a+b}{c}} + af^{\frac{a+b}{c}})^c}, \tag{31}$$

with $a = 3$, $b = 1.51$, $c = 2.18$, $f$ the frequency and with peak frequency

$$f_p = 5.28\cdot 10^{-4}\frac{T_{\rm f}}{100}\left(\frac{g_*}{100}\right)^{1/6}\frac{1}{2\pi R_* H_{\rm f}}. \tag{32}$$

Second, following the prescription of [16], the contribution of sound waves gives the following GW spectrum

$$\frac{d\Omega_{sw}h^2}{dln(f)} = \begin{cases} 0.678h^2F_{\rm sw}G\tilde{\Omega}_{\rm sw}C_f, & \text{if} \quad \frac{H_{\rm f}R_*}{K^{1/2}} > 1 \\ 0.678h^2F_{\rm sw}\bar{G}\tilde{\Omega}_{\rm sw}C_f, & \text{if} \quad \frac{H_{\rm f}R_*}{K^{1/2}} < 1 \end{cases}, \tag{33}$$

where $G = K^2H_{\rm f}R_*/c_s$ and $\bar{G} = K^{3/2}(H_{\rm f}R_*/c_s)^2$ with $c_s$ the speed of sound and with

$$K \approx \frac{3}{4}\frac{k_{\rm sw}\alpha}{1+\alpha}, \quad k_{\rm sw} = k_{\rm fluid}\frac{\alpha}{0.73+0.083\sqrt{\alpha}+\alpha}, \tag{34}$$

where for the case of runaway regime we have to substitute $\alpha$ with $\alpha_\infty$. The factor $F_{\rm sw}$ is $F_{\rm sw} = 3.57\cdot 10^{-5}(100/g_*)^{1/3}$ and the spectral shape is numerically found to be

$$C(s) = s^3\left(\frac{7}{4+3s^2}\right)^{7/2}, \quad s \equiv \frac{f}{f_p}, \tag{35}$$

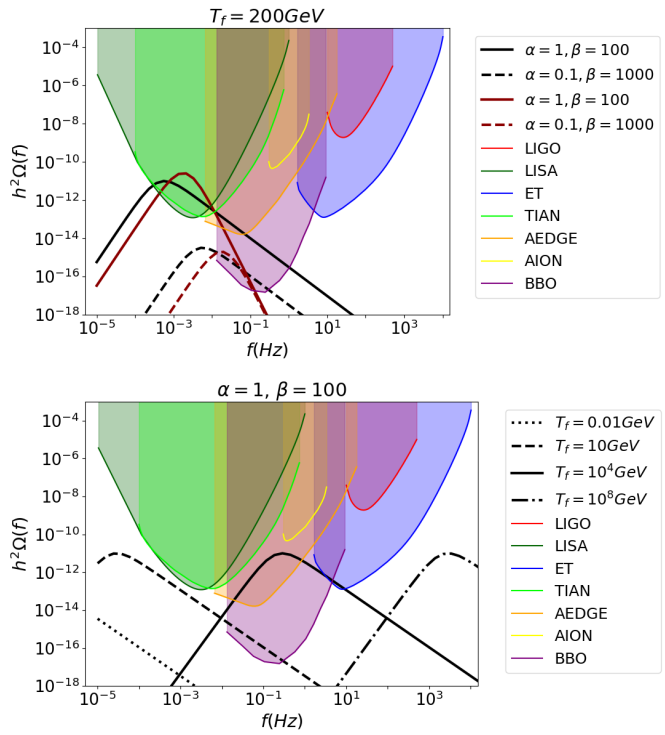


FIG. 6. Upper panel: GW spectra for a fixed $T_{\rm f}$, being the ones presented in red lines for cases in the terminal velocity regime and the ones presented in black lines for cases in the runaway regime. Lower panel: GW spectra for fixed values of $\alpha, \beta$ in the runaway regime. In both panels we are always taking $\alpha_\infty = 0.001$. The presented values of $\beta$ are in units of $H_{\rm f}$. LIGO [23], LISA [12], ET [10], TIAN [24], AEDGE [25], AION [26] and BBO [11] sensitivity curves are also presented.

with peak frequency

$$f_p \simeq 26 \cdot 10^{-6} \frac{1}{H_{\rm f} R_*} \frac{z_p}{10} \frac{T_{\rm f}}{100\,{\rm GeV}} \left(\frac{g_*}{100}\right)^{1/6} {\rm Hz}, \qquad (36)$$

where the peak angular frequency $z_p = (kR_*)_{\rm max}$ is generally around 10. Last, numerical simulations give $\Omega_{\rm sw} \approx 10^{-2}$.

Once all these equations are known, we can derive the GW spectrum for some typical values of the parameters. In Figure (6), we presented the GW spectra for different values of $\alpha, \beta$ as well as for different values of $T_{\rm f}$, fixing $\alpha_\infty = 0.001$. We note that the presented values of $\beta$ are in units of $H_{\rm f}$. We see how this signal could be detected by some of the future experiments, especially when the parameters taken correspond to a PT in the electroweak scale. Since the peak frequency is linearly dependent on $T_{\rm f}$, the spectrum is quite sensitive to it, so large variations of this parameter take the signal out of the current observation range of GWs detectors.

## V. CONCLUSIONS

In this MSc thesis we have studied the DM production mechanism known as BE [9], deriving the DM density produced for different interaction models as well as the associated density parameter, whose value is known from CMB observations [1]. The BE mechanism is fundamentally based on a FOPT in the early universe. The regions in which the transition has already occurred define bubbles within which the symmetry is spontaneously broken, with the field undergoing the transition ($\Phi$) having a non-zero VEV. Thus, the expansion of the bubbles excites the coupling between $\Phi$ and the DM candidate giving rise to $h$ decays in our DM candidate ($\phi$). Therefore, we have studied DM production in this paradigm taking both $\Phi$ and $\phi$ as scalar fields with an interaction $\mathcal{L} \sim \phi^2 \Phi^n$. This way, in Section III we have computed the expressions for $\Omega_{\rm BE} h^2$ for the cases $n = 2, 3, 4$.

First, for $n = 2$ we have essentially reproduced the results presented in [9]. For parameter values corresponding to a PT on the electroweak scale, being the bubbles produced in the runaway regime, there is a wide range of values of the candidate's mass as well as the coupling constant that allow agreement with the observational value. In addition, the model allows very high $M$ values, typically forbidden in other types of mechanisms. However, for a non-relativistic expansion of the bubbles, the abundance is suppressed, constraining the model. Moreover, the density parameter is very sensitive to final temperatures higher than the nucleation temperature, which reduces the parameter space in agreement with observations when $T_{\rm f} > T_{\rm n}$. Therefore, although this case presents interesting results at the electroweak scale, it requires a fine tuning of the transition parameters.

Secondly, a coupling with $n = 3, 4$ has been studied, where the interaction term of the Lagrangian is non-renormalizable, as usual in effective field theories. In both cases, the expressions of the density parameter are proportional to powers of $\gamma_w$ in the ultra-relativistic limit. This dependence becomes greater the larger the dimension of the interaction term in the Lagrangian, from which we infer that for even larger dimensions this dependence will keep growing. This allows great freedom in the parameters. Since we can always take a sufficiently high $\gamma_w$, it is mathematically possible to find agreement with observations for large values of the energy scale up to which the theory es valid, $\Lambda$, the candidate's mass or the final temperature, which would otherwise be excluded. On the other hand, the larger $n$ the better the tolerance to $T_{\rm f}/T_{\rm n} > 1$. This is again positive, since in some types of PTs the final temperature becomes much higher than the nucleation temperature, which in the case of $n = 2$ was rather restricted. Therefore, in general, the stronger the coupling, the more freedom we have in the rest of the parameters, which allows greater freedom in the type of PT that gives rise to this mechanism.

Finally, in Section IV, the GW spectrum associated

with the PT is presented, this being one of the most interesting characteristics of this type of phenomena and therefore also of the mechanism presented. As we have seen, this spectrum has two main contributions: one due to the collision of the bubbles [18] and the other due to the sound waves produced in the plasma [16], whose expressions are obtained from different types of simulations. Thus, the spectrum depends mainly on the transition parameters $\alpha, \beta, T_{\rm f}$ and $v_w$. In order to make this study as general as possible, we have not presented a particular potential for the PT, and consequently we have presented the spectrum for some benchmark values, being able to calculate these parameters once the potential of interest is specified. In this way, it has been seen how for a transition in the electroweak scale this signal could be detected by future experiments such as ET or DECIGO, which would be an enormous source of information about the mechanisms of DM production.

We thus conclude that the BE mechanism constitutes a model of DM to be taken into account. Although in its simplest version the range of possible PTs is restricted, the higher the dependence on the field undergoing the transition in the coupling, the more freedom we find. In addition, the model gives rise to a spectrum of GWs that could be detected in the future. In further studies, it would be of interest to treat other variants of the mechanism, taking $\mathcal{L}_{int} \sim \phi^m h^n$ interaction terms that allow a decay to more than two particles and could give access to other regions of the parameter space. Similarly, fermionic particles could be considered instead of bosonic particles, for which we may expect results similar to those presented in this work.


[1] N. Aghanim *et al.* (Planck), Planck 2018 results. VI. Cosmological parameters, Astron. Astrophys. **641**, A6 (2020), [Erratum: Astron.Astrophys. 652, C4 (2021)], arXiv:1807.06209 [astro-ph.CO].

[2] G. Bertone, D. Hooper, and J. Silk, Particle dark matter: Evidence, candidates and constraints, Phys. Rept. **405**, 279 (2005), arXiv:hep-ph/0404175.

[3] G. Steigman and M. S. Turner, Cosmological Constraints on the Properties of Weakly Interacting Massive Particles, Nucl. Phys. B **253**, 375 (1985).

[4] C. B. Adams *et al.*, Axion Dark Matter, in *Snowmass 2021* (2022) arXiv:2203.14923 [hep-ex].

[5] M. Srednicki, R. Watkins, and K. A. Olive, Calculations of Relic Densities in the Early Universe, Nucl. Phys. B **310**, 693 (1988).

[6] K. Griest and M. Kamionkowski, Unitarity Limits on the Mass and Radius of Dark Matter Particles, Phys. Rev. Lett. **64**, 615 (1990).

[7] D. N. Schramm, Phase Transitions and Dark Matter Problems, Nucl. Phys. B **252**, 53 (1985).

[8] M. Hindmarsh *et al.*, Phase transitions in the early universe, SciPost Phys. Lect. Notes **24**, 1 (2021), arXiv:2008.09136 [astro-ph.CO].

[9] A. Azatov, M. Vanvlasselaer, and W. Yin, Dark Matter production from relativistic bubble walls, JHEP **03**, 288, arXiv:2101.05721 [hep-ph].

[10] M. Punturo *et al.*, The Einstein Telescope: A third-generation gravitational wave observatory, Class. Quant. Grav. **27**, 194002 (2010).

[11] K. Yagi and N. Seto, Detector configuration of DECIGO/BBO and identification of cosmological neutron-star binaries, Phys. Rev. D **83**, 044011 (2011), arXiv:1101.3940 [astro-ph.CO].

[12] P. LISA Collaboration, Amaro-Seoane *et al.*, Laser Interferometer Space Antenna, . (2017), arXiv:1702.00786 [astro-ph.IM].

[13] C. Caprini *et al.*, Science with the space-based interferometer eLISA. II: Gravitational waves from cosmological phase transitions, JCAP **04**, 001, arXiv:1512.06239 [astro-ph.CO].

[14] J. Ellis, M. Lewicki, and J. M. No, On the Maximal Strength of a First-Order Electroweak Phase Transition and its Gravitational Wave Signal, JCAP **04**, 003, arXiv:1809.08242 [hep-ph].

[15] D. Bodeker and G. D. Moore, Electroweak Bubble Wall Speed Limit, JCAP **05**, 025, arXiv:1703.08215 [hep-ph].

[16] M. Hindmarsh, S. J. Huber, K. Rummukainen, and D. J. Weir, Shape of the acoustic gravitational wave power spectrum from a first order phase transition, Phys. Rev. D **96**, 103520 (2017), [Erratum: Phys.Rev.D 101, 089902 (2020)], arXiv:1704.05871 [astro-ph.CO].

[17] C. Caprini *et al.*, Detecting gravitational waves from cosmological phase transitions with LISA: an update, JCAP **03**, 024, arXiv:1910.13125 [astro-ph.CO].

[18] D. Cutting, M. Hindmarsh, and D. J. Weir, Gravitational waves from vacuum first-order phase transitions: from the envelope to the lattice, Phys. Rev. D **97**, 123513 (2018), arXiv:1802.05712 [astro-ph.CO].

[19] A. Azatov and M. Vanvlasselaer, Bubble wall velocity: heavy physics effects, JCAP **01**, 058, arXiv:2010.02590 [hep-ph].

[20] O. Gould, S. Sukuvaara, and D. Weir, Vacuum bubble collisions: From microphysics to gravitational waves, Phys. Rev. D **104**, 075039 (2021), arXiv:2107.05657 [astro-ph.CO].

[21] M. Hindmarsh, S. J. Huber, K. Rummukainen, and D. J. Weir, Gravitational waves from the sound of a first order phase transition, Phys. Rev. Lett. **112**, 041301 (2014), arXiv:1304.2433 [hep-ph].

[22] J. R. Espinosa, T. Konstandin, J. M. No, and G. Servant, Energy Budget of Cosmological First-order Phase Transitions, JCAP **06**, 028, arXiv:1004.4187 [hep-ph].

[23] J. Aasi *et al.* (LIGO Scientific), Advanced LIGO, Class. Quant. Grav. **32**, 074001 (2015), arXiv:1411.4547 [gr-qc].

[24] J. Mei *et al.* (TianQin), The TianQin project: current progress on science and technology, PTEP **2021**, 05A107 (2021), arXiv:2008.10332 [gr-qc].

[25] Y. A. El-Neaj *et al.* (AEDGE), AEDGE: Atomic Experiment for Dark Matter and Gravity Exploration in Space, EPJ Quant. Technol. **7**, 6 (2020), arXiv:1908.00802 [gr-qc].

[26] L. Badurina *et al.*, AION: An Atom Interferometer Observatory and Network, JCAP **05**, 011, arXiv:1911.11755 [astro-ph.CO].